0D and 2D: The Cases of Phenylethylammonium Tin Bromide Hybrids

Liang-Jin Xu,[†] Haoran Lin,[†] Sujin Lee,[†] Chenkun Zhou,[‡] Michael Worku,[§] Maya Chaaban,[†] Qingquan He,[†] Anna Plaviak,[†] Xinsong Lin,[†] Banghao Chen,[†] Mao-Hua Du,[£] and Biwu Ma*[,†,‡,§]

[†]Department Department of Chemistry and Biochemistry, Florida State University Tallahassee, Florida 32306, United States

[‡]Department of Chemical and Biomedical Engineering, FAMU-FSU College of Engineering Tallahassee, Florida 32310, United States

[§]Materials Science and Engineering Program, Florida State University Tallahassee, Florida 32306, United States

[£]National High Magnetic Field Laboratory, Florida State University, Tallahassee, Florida 32310, United States

ABSTRACT: Tin halide perovskites and perovskite-related materials have emerged as promising lead-free hybrid materials for various optoelectronic applications. While remarkable progress has been achieved in the development of organic tin halide hybrids with diverse structures and controlled dimensionalities at the molecular level, some controversial results have been reported recently that need to be addressed. For instance, different photophysical properties have been reported for two-dimensional (2D) $(PEA)_2SnBr_4$ (PEA = Phenylethylammonium) by several groups with distinct emission peaks at around 468 and 550 nm. Here we report our efforts on the synthesis of phenylethylammonium tin bromide hybrids with 0D (zero-dimensional) and 2D structures, and characterizations of their structural and photophysical properties. 0D $[(PEA)_4SnBr_6][(PEA)Br]_2[CCl_2H_2]_2$ was found to exhibit strong yellow emission peaked at 566 nm with a photoluminescence quantum efficiency (PLQE) of ~ 90 %, while 2D $(PEA)_2SnBr_4$ had weak emission peaked at 470 nm with a PLQE of < 0.1%. Interestingly, 0D $[(PEA)_4SnBr_6][(PEA)Br]_2[CCl_2H_2]_2$ can be converted into 2D $(PEA)_2SnBr_4$ upon drying, which would return to 0D $[(PEA)_4SnBr_6][(PEA)Br]_2[CCl_2H_2]_2$ upon the addition of dichloromethane. Powder X-Ray diffraction results confirmed the reversible transformation between 0D and 2D structures. DFT calculations showed that excitons in 0D $[(PEA)_4SnBr_6][(PEA)Br]_2[CCl_2H_2]_2$ are highly localized, resulting in a highly Stokes shifted broadband emission; while delocalized electronic states in 2D $(PEA)_2SnBr_4$ result in a weaker exciton binding, a higher exciton mobility, and a higher nonradiative decay.

Lead-free metal halide perovskites and hybrids have received increasing interests in recent years for various optoelectronic applications, ranging from solar cells, [1-5] to light-emitting diodes (LEDs)[6-12] and sensors.[13-16] Tin based perovskites and hybrids are of particular interest, considering their low toxicity, tunability of optoelectronic properties[17-20] and synthetic control of structure dimensionalities.[10, 11, 21-27] In this regard, highly efficient solar cell based on $ASnI_3$ (A = CH_3NH_3, $CH(NH_2)$ and Cs) perovskites have been demonstrated, [1, 4 28-31] which however exhibit poor stability due to the easy oxidation of Sn(II), hindering their practical exploitation.[28-30, 32] Low-dimensional tin halide hybrids have shown higher stability than 3D tin halide perovskites due to better protection of photoactive tin halide species by organic cations.[12, 21, 22, 24, 26]

Recently, remarkable progress has been achieved on the development and application of low dimensional organic tin halide hybrids. For instance, our group has investigated 0D and 1D organic tin halide hybrids with distinct photophysical properties, and the use of 0D tin halide hybrids as down conversion phosphor for optically pumped white LEDs.[21, 22] Kovalenko and coworkers have demonstrated the use of 0D tin halide hybrids for scintillation, thermometry, and thermography.[13, 15] More recently, 2D organic tin halide hybrids have been reported by several groups, in which different organic cations were used for the synthesis, including phenylethylammonium(PEA),[23, 24] oleyammonium[26] and octylammonium.[33] Interestingly, controversial results have appeared in these reports. On the one hand, several groups have shown strong yellow/orange emissions from 2D tin halide hybrids,[26, 33] e.g. 2D A_2SnBr_4 (A = oleyammonium, octylammonium) reported by Rogach's and Deng's groups, which are indeed very similar to the emissions of previously reported 0D tin halide hybrids.[6, 12, 21, 22] On the other hand, distinct emissions peaked at 468 and 550 nm with low PLQEs were observed for 2D tin halide hybrids, as reported by Haque's and Chou's groups.[23, 24] It is noticed that all these tin bromide hybrids have the same absorption at around 440 nm. Questions have therefore arisen, i) what emissions 2D tin

halide hybrids should have, and ii) is it possible that those strong yellow/orange emissions are indeed from 0D not 2D. To

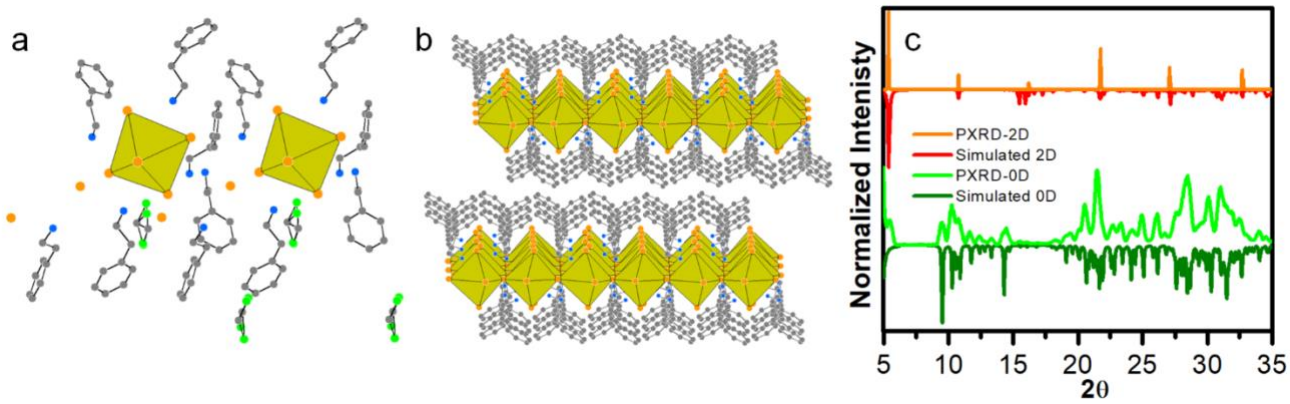

Figure 1. Views of single crystal structures of 0D $[(PEA)_4SnBr_6][(PEA)Br]_2[CCl_2H_2]_2$ (a) and 2D $(PEA)_2SnBr_4$ (b) (Sn red, Br orange, Cl green, N blue, C gray; hydrogen atoms were hidden for clarity). (c) PXRD patterns of 0D (bottom) and 2D (up) and the corresponding simulated peaks from single crystal structures.

answer these questions, a convincible approach needs to be developed to reveal the origins of the emissions of these 2D organic tin bromide hybrids. Making high quality single crystals and investigating their photophysical properties in different environments could be a reliable way to address this controversy.

Here we report the synthesis and characterization of single crystalline 0D and 2D phenylethylammonium tin halide hybrids, $[(PEA)_4SnBr_6][(PEA)Br]_2[CCl_2H_2]_2$ and $(PEA)_2SnBr_4$. By synthetically controlling the reaction conditions, single crystals could be prepared for both 0D and 2D organic tin bromide hybrids, with high yield and excellent reproducibility. It was found that 0D $[(PEA)_4SnBr_6][(PEA)Br]_2[CCl_2H_2]_2$ exhibited strong yellow emission with a high PLQE of ~ 90%, and 2D $(PEA)_2SnBr_4$ had little-to-no emission. Moreover, the emissive 0D $[(PEA)_4SnBr_6][(PEA)Br]_2[CCl_2H_2]_2$ could be converted into 2D $(PEA)_2SnBr_4$ upon drying, and the transformation could be reversed in the presence of dichloromethane (DCM), as verified by PXRD, X-ray photoelectron spectroscopy (XPS) and absorption. DFT calculations show that the strongly Stokes shifted emission of 0D $[(PEA)_4SnBr_6][(PEA)Br]_2[CCl_2H_2]_2$ is a result of the strong local structural distortion at the excited state, while delocalized electronic states in 2D $(PEA)_2SnBr_4$ should lead to a weaker exciton binding, which lowers the radiative recombination rate, and a higher exciton mobility, increasing the probability for an exciton to encounter defects. Our findings reveal the structure-property relationships and clarify the luminescence mechanisms for low-dimensional phenylethylammonium tin bromide hybrids.

Scheme 1. The synthesis of 0D and 2D phenylethylammonium Sn bromide hybrids.

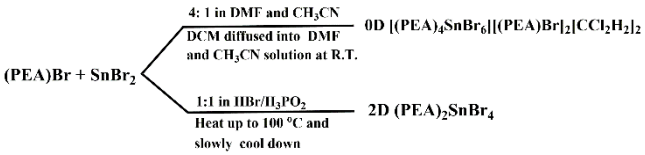

As illustrated in Scheme1 and Figure S1a, single crystals of 0D and 2D tin bromide hybrids can be formed by controlling the reaction conditions and ratios of reactants. Specifically, 0D $[(PEA)_4SnBr_6][(PEA)Br]_2[CCl_2H_2]_2$ single crystals were synthesized by diffusing DCM into the mixture solution of N,N-dimethylformamide (DMF) and acetonitrile containing $SnBr_2$ and PEABr with the ratio of 1:4 in a N_2-filled glovebox. 2D $(PEA)_2SnBr_4$ single crystals were acquired by slowly cooling down the heated HBr solution containing $SnBr_2$ and PEABr with the ratio of 1:2, here extra H_3PO_2 was introduced to prevent the oxidation of Sn(II). Single crystal structures were determined using SCXRD and the corresponding bond distance and angles are listed in table S1, S2 and S3. As show in Figure1a, 0D $[(PEA)_4SnBr_6][(PEA)Br]_2[CCl_2H_2]_2$ adopt a monoclinic space group (Cc), where the isolated $SnBr_6$ octahedrons are surrounded by PEA cations, bromide ions, and DCM molecules. This structure is analogous to our previously reported 0D $(C_4N_2H_{14}Br)_4SnBr_6$. The average Sn-Br bond distance (2.992 Å) in $[(PEA)_4SnBr_6][(PEA)Br]_2[CCl_2H_2]_2$ is comparable to that in $(C_4N_2H_{14}Br)_4SnBr_6$ (3.042 Å).[12] Figure 1b shows the structure of 2D $(PEA)_2SnBr_4$, similar to that of $(PEA)_2PbBr_4$,[34] in which a layer of corner-sharing $SnBr_6$ octahedra is sandwiched between layers of PEA cations with the average bond distance of Sn-Br (3.003 Å). The powder X-ray diffraction (PXRD) patterns of 0D and 2D tin bromide hybrids display the same features as the simulated patterns from SCXRD data (Figure 1c), suggesting the uniform crystal structure of as-prepared phenylethylammonium tin bromide hybrids. The PXRD patterns of 2D $(PEA)_2SnBr_4$ show a periodic diffraction peaks with regular spacings at 5.38°, 10.78°, 16.20°, 21.73°, 27.08°, and 32.78°, which could be assigned to the (001), (002), (003) (004), (005) and (006) lattice planes, similar to those of previously reported 2D layered metal halide perovskites.[23, 24] The thermal stability and composition of these tin bromide hybrids were further characterized by thermogravimetric analysis, with results shown in Figure S2. It was found that decomposition of 0D $[(PEA)_4SnBr_6][(PEA)Br]_2[CCl_2H_2]_2$ started at around 50 °C and a 10% reduction of weight was observed after the temperature reaching 120 °C. This weight loss matches well with the mass ratio of DCM that could escape from the crystal lattice during the heating process. 2D $(PEA)_2SnBr_4$ shows better thermal stability than 0D $[(PEA)_4SnBr_6][(PEA)Br]_2[CCl_2H_2]_2$, without change of weight until 210 °C.

Figure 2a shows the images of the 0D and 2D single crystals under ambient light and UV lamp irradiation (365 nm). 0D

$[(PEA)_4SnBr_6][(PEA)Br]_2[CCl_2H_2]_2$ single crystals were colorless under ambient light and become highly emissive upon UV (365 nm) irradiation, whereas, 2D $(PEA)_2SnBr_4$ single crystals were almost non-emissive under the same UV irradiation. Photophysical properties of 0D $[(PEA)_4SnBr_6][(PEA)Br]_2[CCl_2H_2]_2$ and 2D $(PEA)_2SnBr_4$ were further characterized using UV-vis absorption spectroscopy, as well as steady-state

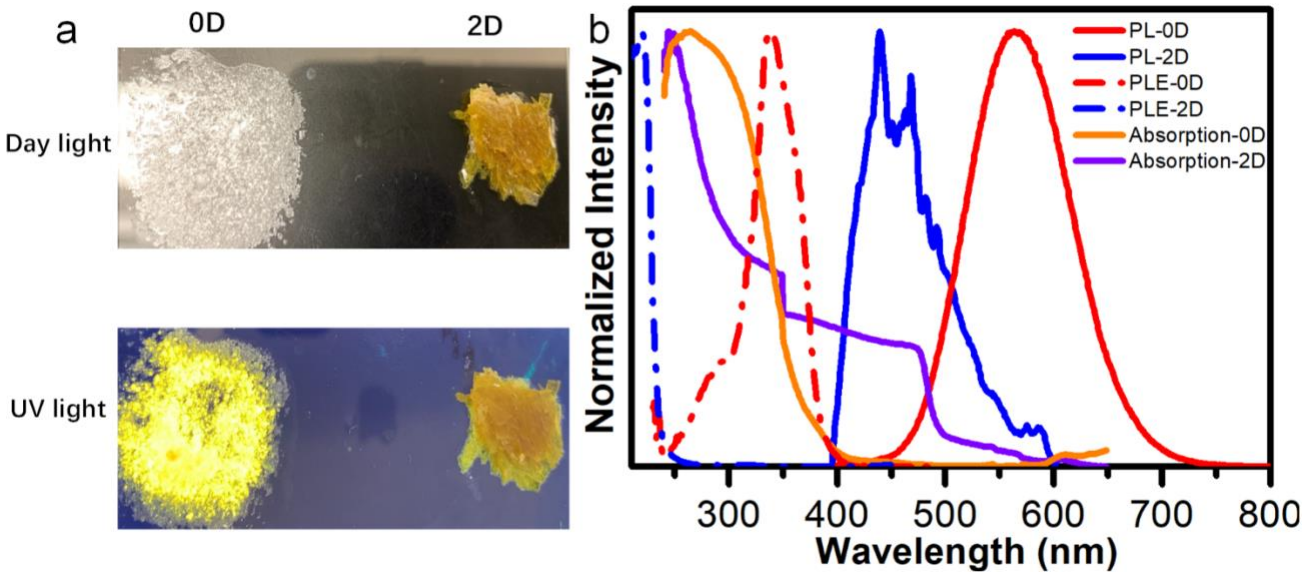

Figure 2. (a) The images of 0D (left) and 2D (right) under day light and UV light. (b) Absorption, excitation and emission of 0D and 2D.

photoluminescence spectroscopy. As shown in Figure 2b, 0D $[(PEA)_4SnBr_6][(PEA)Br]_2[CCl_2H_2]_2$ single crystals possess an intense absorption peaked at 304 nm with a shoulder at around 330 nm. Upon UV irradiation, 0D $[(PEA)_4SnBr_6][(PEA)Br]_2[CCl_2H_2]_2$ single crystals exhibit a strong emission peaked at 566 nm with a PLQE of 89.5% and a long decay lifetime of 2.7 μs (Figure S3) at room temperature. This strongly Stokes shifted broadband emission with a full width at half maximum (FWHM) of 112 nm is almost identical to that of previous reported 0D $(C_4N_2H_{14}Br)_4SnBr_6$, which could be attributed to excited state structural distortion of individual tin bromide octahedrons.[12] In contrast, the emission of 2D $(PEA)_2SnBr_4$ single crystals peaked at around 470 nm is extremely weak with a PLQE of < 0.1%. A strong overlap between the emission and absorption was observed, which is not surprising as 2D layered metal halides often have delocalized electronic states, favoring the formation of weakly bound free excitons. These optical properties of 2D $(PEA)_2SnBr_4$ are consistent with those reported by Lanzetta et al.[24] In addition, distinct excitation spectra were observed on these two hybrids.

Unlike previously reported 0D organic tin bromide hybrids with good stability, fresh 0D $[(PEA)_4SnBr_6][(PEA)Br]_2[CCl_2H_2]_2$ single crystals prepared here are not stable, which could turn into non-emissive powders after exposing in ambient conditions for several minutes, as shown in Figure 3a. X-ray photoelectron spectroscopy (XPS) was used to characterize the non-emissive powders, with results shown in Figure S4. Pronounced shifts of the binding energies of $Sn3d_{3/2}$ and $Sn3d_{5/2}$ were observed, as compared to those of emissive 0D samples, suggesting changes of coordination environments for Sn. More interestingly, the non-emissive powders could return to emissive powders once drops of DCM were introduced, as shown in Figure 3a (also see procedure video in the Supporting Information). The change of photophysical properties were monitored during the transformation. As shown in Figure 3b. The fresh 0D $[(PEA)_4SnBr_6][(PEA)Br]_2[CCl_2H_2]_2$ samples had a strong emission peaked at 566 nm with a PLQE of ~ 90 %, which was quenched after drying for several minutes. Meanwhile, a new weak emission emerged at around 470 nm with a PLQE of less than 0.1%. Upon introducing DCM to the dried samples, the emission at 566 nm re-emerged with a high PLQE of 85.3 %, almost the same as that of fresh 0D $[(PEA)_4SnBr_6][(PEA)Br]_2[CCl_2H_2]_2$ samples. Similar phenomenon was observed in UV-vis absorption as shown in Figure 3b and Figure S5. We therefore suggest that a solvent-induced structure transformation exists between 0D and 2D tin bromide hybrids in the presence/absence of DCM, as shown in Scheme S1.

To validate the reversible transformation between 0D and 2D hybrids, PXRD was performed. At the beginning, we chose the powders of 0D to trace the transformation. As shown in Figure S6, two group peaks belonging to 0D and 2D could be observed in the pristine 0D powders. This is not surprising as the 0D in the form of powder could transfer into 2D rapidly. While the 0D patterns disappear completely after the sample being exposed in ambient conditions for 10 mins, they could reemerge once processed with DCM. To avoid the influence from rapid escaping of solvent, PXRD was conducted on fresh $[(PEA)_4SnBr_6][(PEA)Br]_2[CCl_2H_2]_2$ single crystals wrapped by Paratone-N oil. As shown in Figure 3c. the diffraction patterns of the 0D crystal are identical to those from simulation of SCXRD results. After aging for 3 days, the diffraction patterns of 0D single crystals disappeared, and peaks for 2D $(PEA)_2SnBr_4$ and PEABr emerged. The diffraction patterns for 0D $[(PEA)_4SnBr_6][(PEA)Br]_2[CCl_2H_2]_2$ reappear upon dipping the aged single crystals into DCM solution for several minutes. The recovered peak intensities were weaker as compared to those of fresh 0D $[(PEA)_4SnBr_6][(PEA)Br]_2[CCl_2H_2]_2$ single crystals, which could be due to imperfect crystallization.

Density functional theory (DFT) calculations were conducted on the 0D and 2D structures to gain a deeper insight into the photophysics of the low dimensional tin bromide hybrids. (see computational methods in Supporting Information) As shown in Figure 4a, the electronic structure of 0D $[(PEA)_4SnBr_6][(PEA)Br]_2[CCl_2H_2]_2$ displays small dispersions for both valence and the conduction bands. The valence band is derived from the antibonding orbital of Sn-5s and Br-4p while the conduction band is made up of orbitals from organic molecules and the anti-bonding orbital of Sn-5p and Br-4p (see Figure 4c). The flatness of these bands suggests that the electronic

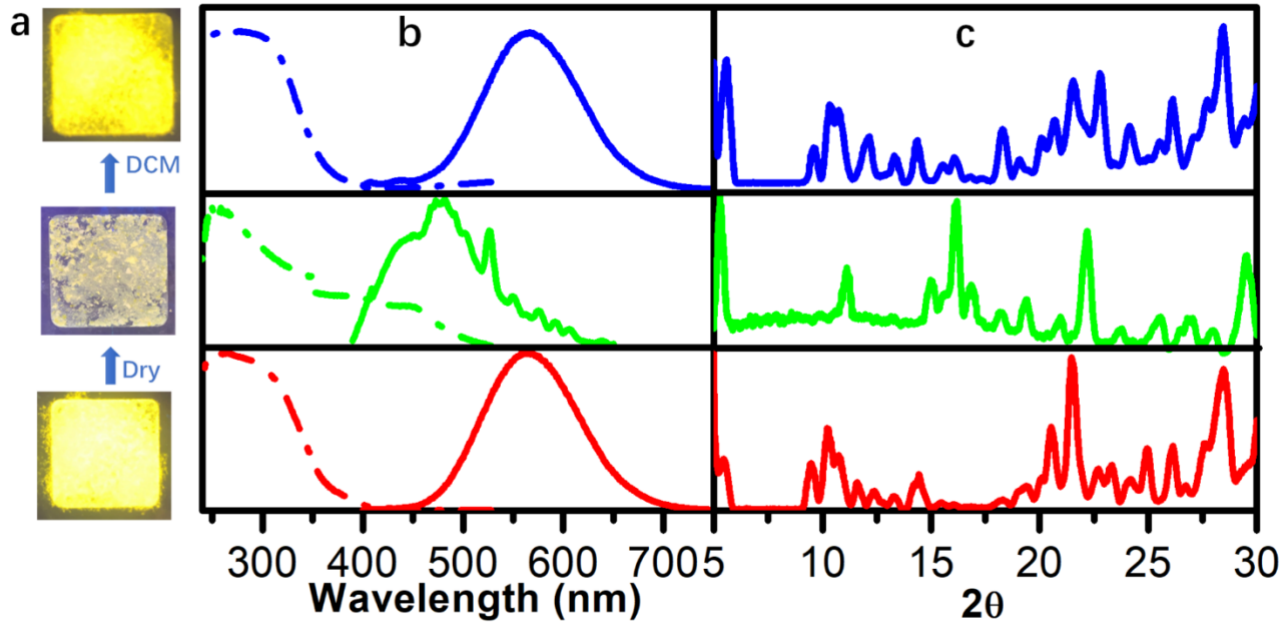

Figure 3. (a) Illustration of phase transformation between 0D and 2D (bottom to up) under UV light. (b) PL and absorption changes during the transformation (bottom to up). (c) PXRD based on 0D single crystal (bottom to up).

states are highly localized and the intermolecular coupling is negligible, therefore, there is nearly no electronic band formation between $SnBr_6$. Thus, the photoluminescence should result from individual $SnBr_6$. The band gap at the Γ point, calculated at the PBE level, is 3.11 eV, which is underestimated due to the well-known band gap error in the PBE calculation. Although the electronic states at the conduction band minimum (CBM) are from organic molecules, the strong coulomb binding leads to the localization of the exciton within a $SnBr_6$ molecule. The exciton wavefunction is similar to those found in other 0D organic metal halides containing SnX_6 and PbX_6 molecules (X = halogen ions).[35, 36] The hole is localized on a $SnBr_4$ plane while the electron is localized on the two vertical Sn-Br bonds (see Figure S7). The hole centered at the Sn ion contracts the four Sn-Br bonds due to the enhanced coulomb attraction, reducing the average length of these four bonds from 3.00 Å to 2.77 Å (a 7.6 % contraction). The electron localization at the two vertical Sn-Br bonds increases their average bond length from 3.04 Å to 3.55 Å (a 16.7% increase). Such strong localization should lead to an efficient radiative recombination of excitons. The calculated exciton emission energy is 2.16 eV, compared to the peak energy of 2.19 eV in the emission spectrum (Figure 2a). The excellent agreement between the calculated and measured exciton emission energies suggests that the observed yellow emission from 0D $[(PEA)_4SnBr_6][(PEA)Br]_2[CCl_2H_2]_2$ is due to the radiative recombination of excitons localized at isolated $SnBr_6$ molecules.

Compared to 0D $[(PEA)_4SnBr_6][(PEA)Br]_2[CCl_2H_2]_2$, the calculated band structure of 2D $(PEA)_2SnBr_4$ shows much more dispersive valence and conduction bands in directions lying on $SnBr_4$ planes (Figure 4b). The inter-layer electronic coupling is weak as indicated by the flat bands along the Γ-M line, which is perpendicular to the $SnBr_4$ plane. The valence and conduction bands are made up of Sn-5s and Sn-5p orbitals hybridized with Br-4p orbitals, respectively (Figure 4d). The calculated band gap at the Γ point is 1.67 eV by using the PBE functional red-shift compared to 0D, which accords well with the absorption of 0D and 2D hybrids. The reduced band gap in 2D $(PEA)_2SnBr_4$ as compared to that of 0D $[(PEA)_4SnBr_6][(PEA)Br]_2[CCl_2H_2]_2$ is caused by the more delocalized electronic states and, consequently, wider conduction and valence bands in 2D Sn bromide. The calculated electronic part of the static dielectric constant [high-frequency dielectric constant (ε_∞)] of 2D $(PEA)_2SnBr_4$ is 3.2, higher than that of 0D $(PEA)_4SnBr_6$, which is calculated to be 2.8; this is consistent with the smaller band gap of the former. The lattice part of the static dielectric constant is expected to be significantly larger in 2D $(PEA)_2SnBr_4$ than in 0D $(PEA)_4SnBr_6$ because the lattice polarization is suppressed in a 0D compound without a bonding network. Thus, compared to 0D $(PEA)_4SnBr_6$, the exciton binding in 2D $(PEA)_2SnBr_4$ should be weaker due to the stronger dielectric screening and the mobility which in turn increases the probability of an exciton

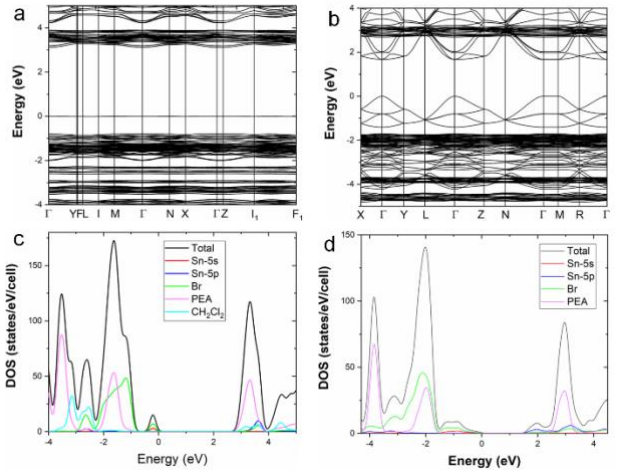

Figure 4. Electronic band structure of 0D $[(PEA)_4SnBr_6][(PEA)Br]_2[CCl_2H_2]_2$ (a) and 2D $(PEA)_2SnBr_4$ (b). Density of states (DOS) of $[(PEA)_4SnBr_6][(PEA)Br]_2[CCl_2H_2]_2$ (c) and 2D $(PEA)_2SnBr_4$ (d) calculated using PBE functionals. Note that the band gap is underestimated due to the well-known band gap error in the PBE calculation. The band structure is calculated based on the primitive cell of structure.

small band gap. The weak exciton binding increases the exciton encountering defects, leading to a higher nonradiative recombination rate.[35] This should contribute to the low PLQE found in 2D $(PEA)_2SnBr_4$.

In summary, we have successfully achieved synthetic control of phenylethylammonium tin bromide hybrids with 0D and 2D structures at the molecular level. Both 0D $[(PEA)_4SnBr_6][(PEA)Br]_2[CCl_2H_2]_2$ and 2D $(PEA)_2SnBr_4$ single crystals could be prepared in high yield by reacting phenylethylammonium bromide with tin bromide under different reaction conditions. Their photophysical properties have been fully characterized, with 0D $[(PEA)_4SnBr_6][(PEA)Br]_2[CCl_2H_2]_2$ exhibiting strong yellow emission with a long decay lifetime, and 2D $(PEA)_2SnBr_4$ displaying little-to-no emission at room temperature. Reversible transformation between 0D and 2D phenylethylammonium tin bromide hybrids was realized in the presence/absence of dichloromethane solvent. The electronic structures of 0D and 2D phenylethylammonium tin bromide hybrids have been investigated by DFT calculations, which help to address the controversial results on luminescent low dimensional organic tin bromide hybrids.

EXPERIMENTAL SECTION

Materials. Tin (II) bromide (99.7%), Phenylethylamine, hydrobromic acid (48 wt% in H_2O) and, hypophosphorous acid solution (H_3PO_2, 50 wt. % in H_2O) were purchased from Sigma-Aldrich. Dimethylformamide (DMF, 99.8 %), Dichloromethane (DCM, 99.9%), Acetonitrile (CH_3CN, 99.8%) was purchased from VWR. All reagents and solvents were used without further purification unless otherwise stated.

Synthesis of phenylethylammonium bromide (PEA)Br. Phenylethylammonium bromide was prepared by adding hydrobromic acid solution (1.74 ml, 15.4 mmol) into Phenylethylamine (2.00 ml, 15.3 mmol) in 100 ml ethanol at 0 °C and stirring for 0.5 h. The white organic salts were obtained (1.5 g) after filtration under vacuum, followed by washing with a suitable amount of ethanol and ethyl ether. The salts were dried and kept in a desiccator for future use.

Growth of 0D $[(PEA)_4SnBr_6][(PEA)Br]_2[CCl_2H_2]_2$ crystals. $SnBr_2$ (2.0 mmol) and PEABr (8.0 mmol) were dissolved in the mixture solution containing 1 ml DMF and 2 ml CH_3CN and then filtered into a small vial to form a clear precursor solution. Then the small vial was putting in a big vial with 10 ml DCM inside. Colorless block crystals could be afforded by leaving the vial to stand for around 3 days. Yield ~ 58 %. All the procedures were carried out in N_2-filled glove box to prevent the oxidation of Sn (II) to Sn (IV).

Growth of 2D $(PEA)_2SnBr_4$ crystals. $SnBr_2$ (2.0 mmol) and PEABr (4.0 mmol) was dissolved in a mixture of HBr (3 ml) and H_3PO_2 (1 ml) solution by heating to 100 °C under constant magnetic stirring and nitrogen flow for about 5 min. Then the solution was left to slowly cool to room temperature to afford yellow flake single crystals. The 2D $(PEA)_2SnBr_4$ crystals were washed with acetone and ethyl ether then dried under reduced pressure. Yield ~ 88 %.

Single crystal X-ray diffraction (SCXRD). Single crystal X-ray data for the 0D and 2D were collected using a Rigaku XtaLAB Synergy-S diffractometer equipped with a HyPix-6000HE Hybrid Photon Counting (HPC) detector and dual Mo and Cu microfocus sealed X-ray source as well as a low-temperature Oxford Cryosystem 800.

Powder X-ray diffraction (PXRD). The PXRD analysis was performed on Panalytical X'PERT Pro Powder X-Ray Diffractometer using Copper X-ray tube (standard) radiation at a voltage of 40 kV and 40 mA, and X'Celerator RTMS detector. The diffraction pattern S was scanned over the angular range of 5-40 degree (2θ) with a step size of 0.02, at room temperature.

PXRD based on powders: The powder of 0D was took out from the mother liquid, loaded to the glass holder and measured on Panalytical X'PERT Pro Powder X-Ray Diffractometer using Copper X-ray tube (standard) radiation at a voltage of 40 kV and 40 mA, and X'Celerator RTMS detector at room temperature. After exposure in ambient condition for 20 mins, the white 0D powder become yellow, then this aged 0D was collected under the same condition. The white powder could be reappeared once dipping several drops of DCM into the yellow powder. And then the PXRD was collected on this white powder.

PXRD based on single crystal: A selected single crystal of 0D hybrids wrapped with paratone-N oil was fished by a cryoloop and mounted to SCXRD machine equipped with an Oxford-Diffraction Cryojet at the temeperature of100K. The data were collected using a Rigaku XtaLAB Synergy-S diffractometer equipped with a HyPix-6000HE Hybrid Photon Counting (HPC) detector and Cu microfocus sealed X-ray source. Then take out the single crystal and leave it to stand for 3 days at ambient conditions, the aged sample was then collected with the same condition. After that, the sample was dipped into DCM solution for several minutes, and then collected the recovered sample on Rigaku XtaLAB Synergy-S diffractometer.

Absorption spectrum measurements. Absorption spectra were measured at room temperature on Cary 5000 UV-Vis-NIR spectrophotometer. Specially, the absorption spectra of original 0D and recovered 0D were recorded by dispersing

them into DCM solvent as they are very easy to transform into 2D without solvent. The absorption spectra of original 2D and aged 0D were recorded by using powders of these materials.

Photoluminescence steady state studies. Steady-state photoluminescence spectra of 0D and 2D were obtained at room temperature on a FS5 spectrofluorometer (Edinburgh Instruments).

Photoluminescence quantum Yield (PLQY). The PLQYs were acquired using a Hamamatsu Quantaurus-QY Spectrometer (Model C11347-11) equipped with a xenon lamp, integrated sphere sample chamber and CCD detector. The PLQEs were calculated by the equation: $\eta QE=IS/(ER-ES)$, in which IS represents the luminescence emission spectrum of the sample, ER is the spectrum of the excitation light from the empty integrated sphere (without the sample), and ES is the excitation spectrum for exciting the sample.

Time-resolved photoluminescence. Time-Resolved Emission data were collected at room temperature using the FS5 spectrofluorometer. The dynamics of emission decay were monitored by using the FS5's time-correlated single-photon counting capability with data collection for 10,000 counts. Excitation was provided by an Edinburgh EPL-360 picosecond pulsed diode laser. The average lifetime was obtained by single-exponential fitting.

X-ray photoelectron spectroscopy (XPS). XPS measurements were carried out using a ULVACPHI, Inc., PHI 5000 VersaProbe II. The survey XPS spectra were recorded with a monochromatic Al Ka source using a 93.9 pass energy and 0.8 eV per step. High-resolution spectra were recorded using a 11.75 pass energy and 0.1 eV per step.

Thermogravimetric analysis (TGA). TGA was carried out using a TA instruments Q50 TGA system. The samples were heated from room temperature (around 22 ^{o}C) to 800 ^{o}C at a rate of 5 ^{o}C min^{-1}, under a nitrogen flux of 100 ml min^{-1}.

[CCDC 1982253-1982254 contains the supplementary crystallographic data for this paper. These data can be obtained free of charge from The Cambridge Crystallographic Data Centre via www.ccdc.cam.ac.uk/data_request/cif.]

ASSOCIATED CONTENT

The Supporting Information is available free of charge via the Internet at http://pubs.acs.org. This file contains details of computational methods and results, crystal growth scheme, material structural and photophysical properties, video of conversion between 2D and 0D.

AUTHOR INFORMATION

Corresponding Author

* bma@fsu.edu.

Author Contributions

All authors have given approval to the final version of the manuscript.

Notes

The authors declare no competing financial interest.

ACKNOWLEDGMENT

The authors acknowledge the supports from the National Science Foundation (DMR-1709116), the Air Force Office of Scientific Research (AFOSR) (17RT0906), and the FSU Office of Research. M. -H. Du was supported by the U. S. Department of Energy, Office of Science, Basic Energy Sciences, Materials Science and Engineering Division.

REFERENCES

1. Hao, F.; Stoumpos, C. C.; Cao, D. H.; Chang, R. P. H.; Kanatzidis, M. G., Lead-free solid-state organic-inorganic halide perovskite solar cells. *Nature Photonics* **2014,** 8, (6), 489-494.
2. Harikesh, P. C.; Mulmudi, H. K.; Ghosh, B.; Goh, T. W.; Teng, Y. T.; Thirumal, K.; Lockrey, M.; Weber, K.; Koh, T. M.; Li, S.; Mhaisalkar, S.; Mathews, N., Rb as an Alternative Cation for Templating Inorganic Lead-Free Perovskites for Solution Processed Photovoltaics. *Chemistry of Materials* **2016,** 28, (20), 7496-7504.
3. Kim, Y.; Yang, Z.; Jain, A.; Voznyy, O.; Kim, G. H.; Liu, M.; Quan, L. N.; Garcia de Arquer, F. P.; Comin, R.; Fan, J. Z.; Sargent, E. H., Pure Cubic-Phase Hybrid Iodobismuthates AgBi2 I7 for Thin-Film Photovoltaics. *Angew Chem Int Ed Engl* **2016,** 55, (33), 9586-90.
4. Noel, N. K.; Stranks, S. D.; Abate, A.; Wehrenfennig, C.; Guarnera, S.; Haghighirad, A. A.; Sadhanala, A.; Eperon, G. E.; Pathak, S. K.; Johnston, M. B.; Petrozza, A.; Herz, L. M.; Snaith, H. J., Lead-free organic-inorganic tin halide perovskites for photovoltaic applications. *Energ Environ Sci* **2014,** 7, (9), 3061-3068.
5. Park, B. W.; Philippe, B.; Zhang, X.; Rensmo, H.; Boschloo, G.; Johansson, E. M., Bismuth Based Hybrid Perovskites A3Bi2 I9 (A: Methylammonium or Cesium) for Solar Cell Application. *Adv Mater* **2015,** 27, (43), 6806-13.
6. Fu, P.; Huang, M.; Shang, Y.; Yu, N.; Zhou, H. L.; Zhang, Y. B.; Chen, S.; Gong, J.; Ning, Z., Organic-Inorganic Layered and Hollow Tin Bromide Perovskite with Tunable Broadband Emission. *ACS applied materials & interfaces* **2018,** 10, (40), 34363-34369.
7. Wang, Y.; Zou, R.; Chang, J.; Fu, Z.; Cao, Y.; Zhang, L.; Wei, Y.; Kong, D.; Zou, W.; Wen, K.; Fan, N.; Wang, N.; Huang, W.; Wang, J., Tin-Based Multiple Quantum Well Perovskites for Light-Emitting Diodes with Improved Stability. *The journal of physical chemistry letters* **2019,** 10, (3), 453-459.
8. Worku, M.; Tian, Y.; Zhou, C.; Lee, S.; Meisner, Q.; Zhou, Y.; Ma, B., Sunlike White-Light-Emitting Diodes Based on Zero-Dimensional Organic Metal Halide Hybrids. *ACS applied materials & interfaces* **2018,** 10, (36), 30051-30057.
9. Xu, L. J.; Sun, C. Z.; Xiao, H.; Wu, Y.; Chen, Z. N., Green-Light-Emitting Diodes based on Tetrabromide Manganese(II) Complex through Solution Process. *Adv Mater* **2017,** 29, (10).
10. Zhou, C.; Tian, Y.; Yuan, Z.; Lin, H.; Chen, B.; Clark, R.; Dilbeck, T.; Zhou, Y.; Hurley, J.; Neu, J.; Besara, T.; Siegrist, T.; Djurovich, P.; Ma, B., Highly Efficient Broadband Yellow Phosphor Based on Zero-Dimensional Tin Mixed-Halide Perovskite. *ACS applied materials & interfaces* **2017,** 9, (51), 44579-44583.
11.Zhou, C.; Worku, M.; Neu, J.; Lin, H.; Tian, Y.; Lee, S.; Zhou, Y.; Han, D.; Chen, S.; Hao, A.; Djurovich, P. I.; Siegrist, T.; Du, M.-H.; Ma, B., Facile Preparation of Light Emitting Organic Metal Halide Crystals with Near-Unity Quantum Efficiency. *Chemistry of Materials* **2018,** 30, (7), 2374-2378.
12. Zhou, C. K.; Lin, H. R.; Tian, Y.; Yuan, Z.; Clark, R.; Chen, B. H.; van de Burgt, L. J.; Wang, J. C.; Zhou, Y.; Hanson, K.; Meisner, Q. J.; Neu, J.; Besara, T.; Siegrist, T.; Lambers, E.; Djurovich, P.; Ma, B. W.,

Luminescent zero-dimensional organic metal halide hybrids with near-unity quantum efficiency. *Chem Sci* **2018,** 9, (3), 586-593.
13. Morad, V.; Shynkarenko, Y.; Yakunin, S.; Brumberg, A.; Schaller, R. D.; Kovalenko, M. V., Disphenoidal Zero-Dimensional Lead, Tin, and Germanium Halides: Highly Emissive Singlet and Triplet Self-Trapped Excitons and X-ray Scintillation. *Journal of the American Chemical Society* **2019,** 141, (25), 9764-9768.
14. Qian, L.; Sun, Y.; Wu, M.; Li, C.; Xie, D.; Ding, L.; Shi, G., A lead-free two-dimensional perovskite for a high-performance flexible photoconductor and a light-stimulated synaptic device. *Nanoscale* **2018,** 10, (15), 6837-6843.
15. Yakunin, S.; Benin, B. M.; Shynkarenko, Y.; Nazarenko, O.; Bodnarchuk, M. I.; Dirin, D. N.; Hofer, C.; Cattaneo, S.; Kovalenko, M. V., High-resolution remote thermometry and thermography using luminescent low-dimensional tin-halide perovskites. *Nature materials* **2019,** 18, (8), 846-852.
16. Kagan, C. R.; Mitzi, D. B.; Dimitrakopoulos, C. D., Organic-inorganic hybrid materials as semiconducting channels in thin-film field-effect transistors. *Science* **1999,** 286, (5441), 945-947.
17. Lin, H.; Zhou, C.; Tian, Y.; Siegrist, T.; Ma, B., Low-Dimensional Organometal Halide Perovskites. *ACS Energy Letters* **2017,** 3, (1), 54-62.
18. Ning, W.; Gao, F., Structural and Functional Diversity in Lead-Free Halide Perovskite Materials. *Adv Mater* **2019,** 31, (22), e1900326.
19. Zhou, C.; Lin, H.; He, Q.; Xu, L.; Worku, M.; Chaaban, M.; Lee, S.; Shi, X.; Du, M.-H.; Ma, B., Low dimensional metal halide perovskites and hybrids. *Materials Science and Engineering: R: Reports* **2019,** 137, 38-65.
20. Fraccarollo, A.; Canti, L.; Marchese, L.; Cossi, M., First principles study of 2D layered organohalide tin perovskites. *J Chem Phys* **2017,** 146, (23).
21. Zhou, C.; Lin, H.; Shi, H.; Tian, Y.; Pak, C.; Shatruk, M.; Zhou, Y.; Djurovich, P.; Du, M. H.; Ma, B., A Zero-Dimensional Organic Seesaw-Shaped Tin Bromide with Highly Efficient Strongly Stokes-Shifted Deep-Red Emission. *Angew Chem Int Ed Engl* **2018,** 57, (4), 1021-1024.
22. Zhou, C.; Tian, Y.; Wang, M.; Rose, A.; Besara, T.; Doyle, N. K.; Yuan, Z.; Wang, J. C.; Clark, R.; Hu, Y.; Siegrist, T.; Lin, S.; Ma, B., Low-Dimensional Organic Tin Bromide Perovskites and Their Photoinduced Structural Transformation. *Angew Chem Int Ed Engl* **2017,** 56, (31), 9018-9022.
23. Chen, M. Y.; Lin, J. T.; Hsu, C. S.; Chang, C. K.; Chiu, C. W.; Chen, H. M.; Chou, P. T., Strongly Coupled Tin-Halide Perovskites to Modulate Light Emission: Tunable 550-640 nm Light Emission (FWHM 36-80 nm) with a Quantum Yield of up to 6.4. *Adv Mater* **2018,** 30, (20), e1706592.
24. Lanzetta, L.; Marin-Beloqui, J. M.; Sanchez-Molina, I.; Ding, D.; Haque, S. A., Two-Dimensional Organic Tin Halide Perovskites with Tunable Visible Emission and Their Use in Light-Emitting Devices. *ACS Energy Letters* **2017,** 2, (7), 1662-1668.
25. Lin, J. T.; Liao, C. C.; Hsu, C. S.; Chen, D. G.; Chen, H. M.; Tsai, M. K.; Chou, P. T.; Chiu, C. W., Harnessing Dielectric Confinement on Tin Perovskites to Achieve Emission Quantum Yield up to 21. *Journal of the American Chemical Society* **2019,** 141, (26), 10324-10330.
26. Zhang, X.; Wang, C.; Zhang, Y.; Zhang, X.; Wang, S.; Lu, M.; Cui, H.; Kershaw, S. V.; Yu, W. W.; Rogach, A. L., Bright Orange Electroluminescence from Lead-Free Two-Dimensional Perovskites. *ACS Energy Letters* **2018,** 4, (1), 242-248.
27. Dang, Y. Y.; Zhou, Y. A.; Liu, X. L.; Ju, D. X.; Xia, S. Q.; Xia, H. B.; Tao, X. T., Formation of Hybrid Perovskite Tin Iodide Single Crystals by Top-Seeded Solution Growth. *Angew Chem Int Edit* **2016,** 55, (10), 3447-3450.
28. Jokar, E.; Chien, C. H.; Tsai, C. M.; Fathi, A.; Diau, E. W. G., Robust Tin-Based Perovskite Solar Cells with Hybrid Organic Cations to Attain Efficiency Approaching 10%. *Advanced Materials* **2019,** 31, (2).
29. Lee, S. J.; Shin, S. S.; Kim, Y. C.; Kim, D.; Ahn, T. K.; Noh, J. H.; Seo, J.; Seok, S. I., Fabrication of Efficient Formamidinium Tin Iodide Perovskite Solar Cells through SnF(2)-Pyrazine Complex. *Journal of the American Chemical Society* **2016,** 138, (12), 3974-7.
30. Shao, S. Y.; Liu, J.; Portale, G.; Fang, H. H.; Blake, G. R.; ten Brink, G. H.; Koster, L. J. A.; Loi, M. A., Highly Reproducible Sn-Based Hybrid Perovskite Solar Cells with 9% Efficiency. *Advanced Energy Materials* **2018,** 8, (4).
31. Wang, Z. Y.; Ganose, A. M.; Niu, C. M.; Scanlon, D. O., First-principles insights into tin-based two-dimensional hybrid halide perovskites for photovoltaics. *J Mater Chem A* **2018,** 6, (14), 5652-5660.
32. Wang, F.; Ma, J.; Xie, F.; Li, L.; Chen, J.; Fan, J.; Zhao, N., Organic Cation-Dependent Degradation Mechanism of Organotin Halide Perovskites. *Advanced Functional Materials* **2016,** 26, (20), 3417-3423.
33. Wang, A. F.; Guo, Y. Y.; Zhou, Z. B.; Niu, X. H.; Wang, Y. G.; Muhammad, F.; Li, H. B.; Zhang, T.; Wang, J. L.; Nie, S. M.; Deng, Z. T., Aqueous acid-based synthesis of lead-free tin halide perovskites with near-unity photoluminescence quantum efficiency. *Chem Sci* **2019,** 10, (17), 4573-4579.
34. Ma, D.; Fu, Y.; Dang, L.; Zhai, J.; Guzei, I. A.; Jin, S., Single-crystal microplates of two-dimensional organic – inorganic lead halide layered perovskites for optoelectronics. *Nano Research* **2017,** 10, (6), 2117-2129.
35. Han, D.; Shi, H.; Ming, W.; Zhou, C.; Ma, B.; Saparov, B.; Ma, Y.-Z.; Chen, S.; Du, M.-H., Unraveling luminescence mechanisms in zero-dimensional halide perovskites. *Journal of Materials Chemistry C* **2018,** 6, (24), 6398-6405.
36. Shi, H.; Han, D.; Chen, S.; Du, M.-H., Impact of metal ns2 lone pair on luminescence quantum efficiency in low-dimensional halide perovskites. *Physical Review Materials* **2019,** 3, (3), 034604.

TOC